

Fabrication and characterization of a binary diffractive lens for controlling focal distribution

ATSUSHI MOTOGAITO,^{1,*}  YOSUKE IGUCHI,¹ SHUJI KATO,² AND KAZUMASA HIRAMATSU¹

¹Graduate School of Engineering, Mie University, 1577 Kurima-Machiya-Cho, Tsu, Mie 514-8507, Japan

²Faculty of Engineering, Mie University, 1577 Kurima-Machiya-Cho, Tsu, Mie 514-8507, Japan

*Corresponding author: motogaito@elec.mie-u.ac.jp

Received 21 October 2019; revised 18 December 2019; accepted 18 December 2019; posted 19 December 2019 (Doc. ID 381139); published 15 January 2020

We fabricated a binary diffractive lens to control focal distribution, such as intensity distribution, by controlling the focal length and depth of focus. The results revealed changes in the focal length and depth of focus as a function of changes in the ring zone interval ΔR_M at the end of the lens. Similar results were obtained from experiments. The peak position on the optical axis shifts further away from the lens. The half-width in the propagation direction increases with the ΔR_M . These results demonstrate the possibility of controlling the focal distribution using single flat lenses by changing the periodic structure. © 2020 Optical Society of America

<https://doi.org/10.1364/AO.381139>

1. INTRODUCTION

The application of laser beams can be utilized in various fields such as communication, recording, processing, and measurement, owing to their high directivity. Thus, optical elements for controlling laser light have attracted significant research attention. Optical lenses, such as convex lenses and axicon lenses, are often employed to arbitrarily control the distribution of laser light by refraction.

The focal length of a lens is a function of its refractive index and radius of curvature. Cylindrical or ring-shaped beams can be obtained by focusing a laser beam with an axicon lens. A wide variety of beam patterns can be generated through a combination of lenses. When a laser beam is incident on a convex lens, all the light is focused at a single point. In contrast, the wavefront of a laser beam transmitted through an axicon lens is given by a conical surface, with the propagation axis given by the axis of rotational symmetry. A region of high light intensity is generated through interference on the propagation axis. In addition, axicon lenses have a high depth of focus. It is not necessary to implement exact control of the focal length for axicon lenses; their depth of focus is controlled by the size of the apex angle of the conical surface.

Optical lenses are difficult to downsize owing to the presence of curvatures. In contrast, the focal length of diffractive lenses is independent of the refractive index and radius of curvature and can be controlled by the structure formed on the surface of the lens. Thus, diffractive lenses have a greater degree of freedom for controlling the focal length than optical lenses. Furthermore, because diffractive lenses do not have curvatures, they can be made thinner than optical lenses. Moreover,

they can be fabricated with materials in the ultraviolet region [1]. In this paper, we focus on diffractive lenses in this study. Because diffractive lenses can be fabricated using electron-beam lithography, their manufacture is relatively easy to transfer to nanoimprint technology for mass production and for scaling up to the fabrication of large-area structures. Furthermore, it is possible to produce diffractive lenses with thicknesses of the order of a single wavelength.

Diffractive lenses were first developed as a zone plate by Soret [2]. To improve the efficiency of diffraction of light, kinoforms were developed by Lesem *et al.* [3,4]. Subsequently, the development of multilevel diffractive optical elements with a step-shaped cross section led to the development of binary optical elements based on computer-aided design and large-area integration technology [5]. With the structure of multilevel gratings, obtaining optical effects similar to those of kinoforms is possible [6,7]. A subwavelength structure equivalent to a blaze structure was proposed by Lalanne *et al.* [8,9], making it possible to create a lens structure by converting a Fresnel lens into a binary subwavelength structure. In addition, this structure makes it possible to fabricate achromatic diffractive lenses [10].

Previously, we fabricated two types of binary diffractive lenses for controlling the light distribution of light-emitting diodes (LEDs): a binary diffractive convex lens for focusing LED light [1,11] and a binary diffraction concave lens for diffusing LED illumination [12]. Because these lenses contain several submicrometer structures, it is necessary to use electron-beam lithography technology for their fabrication [1,11,12]. Generally, photolithography and nanoimprint technology are recommended for large-area, low-cost mass production.

However, we employed electron-beam lithography to obtain a targeted optimum structure because it does not require a mold or mask.

In laser processing, it is difficult to drill to a high depth at a high aspect ratio with nanometer-order diameters using short-wavelength lasers such as higher-order harmonic YAG lasers, which have typical wavelengths of $\lambda = 532$ nm, 355 nm, etc. This is attributed to the difficulty in controlling the focal length and the depth of focus through the curvature radius of the convex lens or the apex angle of the axicon lens. We designed and fabricated a diffractive lens structure that functions as both a convex lens and an axicon lens on one flat substrate. We call this lens a binary diffractive lens for controlling focal distribution, indicating that it is an optical element with a focal length and depth of focus that can be controlled simultaneously. We simulated and measured the light distribution of the designed structure to confirm the simultaneous control of the focal length and depth of focus.

Axicon lenses with a binary diffractive structure have been previously reported [13–17]. In most previous studies, the focal length of the axicon lens is proportional to the square of the zone radius. However, our proposed structure is the first to our knowledge to function as a hybrid of both a convex lens and an axicon lens on the same substrate by combining a diffractive grating and a diffractive lens. The focal length and depth of focus can be controlled by the phase shift of the first-order diffraction light based on the phase shifts of the diffractive grating and diffractive lens, which are proportional to the zone radius and the square of the zone radius, respectively. Furthermore, most previous studies have primarily focused on the simulation and design of axicon lenses; however, herein we conducted both simulations and experiments. This lens structure is expected to be suitable for obtaining fine drilling patterns for laser processing owing to the accurate control of the focal length and depth of focus.

Theoretically, a Fresnel lens with a sawtooth structure is used to achieve a first-order diffraction efficiency of 100%. However, to prepare a sawtooth structure, the dose amount for electron-beam lithography needs to be changed gradually. Moreover, setting such conditions for electron-beam lithography is extremely difficult. When approximating a sawtooth structure and binarizing it, it can be regarded as equivalent to a sawtooth-shaped refractive index distribution, and it is easy to prepare a binary diffractive lens. By using the features of a binary diffractive lens [18,19] broadband focusing [20], dual focusing [21], and optical vortices [22] can be realized. Recently, metalenses, obtained using metal or dielectric metasurfaces, have been fabricated for realizing various devices [23,24].

In this study, we propose a binary diffractive lens for controlling focal distribution. We notice the phase shift of the first-order diffraction. For most diffractive lenses, the phase shift, which is proportional to the square of the ring radius, is used to focus the incident light on the focal point. However, this method provides only a fixed light focusing characteristic. Our proposed method is a combination of diffractive grating and a diffractive lens, which are proportional to the ring radius and square of the ring radius, respectively. Changing the structure of the lens causes a change in the phase shift, focal length, and depth of focus. Therefore, the focal distribution (intensity

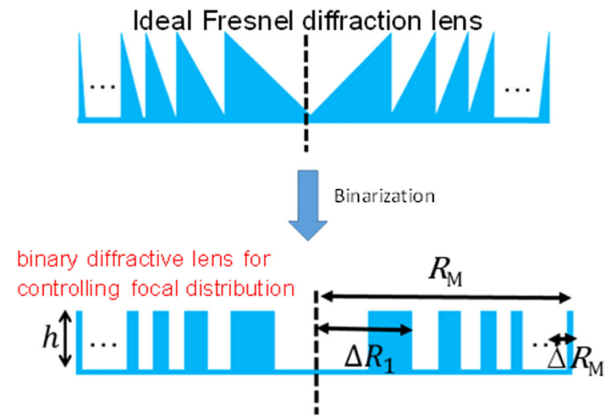


Fig. 1. Schematic diagram of the fabricated lens.

distribution) can be controlled from diffractive lenses to axicon lenses. With this method, if a quadratic polynomial can be used to express the phase shift and other functions of the ring radius, various focal characteristics can be realized.

In this paper, we present our work on the fabrication and characterization of a binary diffractive lens for controlling focal distribution using the phase shift expressed by a quadratic polynomial of the ring radius.

2. DESIGN AND SIMULATION

A. Design Method

We designed a binary diffractive lens with a controllable focus based on an ideal Fresnel diffractive lens that employs both grating and diffractive lenses. Figure 1 shows schematic diagrams of the cross-sectional and top views of the designed lenses. This structure is based on the Fresnel lens and comprises binary structures. Details of the method of conversion from the Fresnel lens structure to the binary structure can be found in [11,12]. In this figure, the annular zone interval ΔR_1 at the center of the initial zone interval and the annular zone interval ΔR_M at the terminal position, representing the M th zone of the lens, are independent variables used in the simulation, where R_M is the radius of the lens. The wavelength of the incident light is $\lambda_0 = 532$ nm. The height of the lens h can be expressed as follows:

$$h = \frac{\lambda_0}{2(n-1)}, \tag{1}$$

where n is the refractive index of the lens medium. This is equivalent to the phase difference in the height direction adjusted to π to eliminate the zeroth-order light.

The phase shift of the first-order diffractive light produced by our proposed lens structure was calculated for a given set of independent parameters: ΔR_1 , ΔR_M , R_{max} , and λ_0 . Its dependence on the zone radius r is given by the following relation:

$$\phi_d(r) = k_0(ar + br^2), \tag{2}$$

where $k_0 = \lambda_0/2\pi$ denotes the wavenumber. The lens in Eq. (2) combines diffractive grating and diffractive lens. The first term represents the phase shift of the first-order diffractive light for the diffractive grating, whereas the second term represents the

phase shift for the diffractive lens. The coefficients a and b are determined by ΔR_1 , ΔR_M , R_M , and λ_0 . The m th zone ring radius r_m is satisfied by the following equation representing the phase difference in the radial direction adjusted to 2π :

$$\phi_d(r_m) = 2\pi m. \quad (3)$$

From Eqs. (2) and (3), r_m is obtained as follows:

$$r_m = \frac{-a + \sqrt{a^2 + 4bm\lambda_0}}{2b}. \quad (4)$$

The annular zone interval Δr_m is expressed as follows:

$$\Delta r_m = r_m - r_{m-1}. \quad (5)$$

From Eq. (5), $\Delta R_1 = \Delta r_1$ and $\Delta R_M = \Delta r_M$. For M , the maximum value of m , ϕ_d , is satisfied with the following equations:

$$\phi_d(R_M) = \frac{2\pi}{\lambda_0}(aR_M + bR_M^2) = 2\pi M, \quad (6)$$

$$aR_M + bR_M^2 = M\lambda_0. \quad (7)$$

Similarly, for $M - 1$,

$$R_{M-1} = R_M - \Delta R_M, \quad (8)$$

$$\phi_d(R_{M-1}) = \frac{2\pi}{\lambda_0}(aR_{M-1} + bR_{M-1}^2) = (M - 1)\lambda_0, \quad (9)$$

$$a(R_M - \Delta R_M) + b(R_M - \Delta R_M)^2 = (M - 1)\lambda_0. \quad (10)$$

Taking the difference between Eqs. (6) and (7), the coefficient of b is obtained as follows:

$$a\Delta R_M + b(2R_M \cdot \Delta R_M - \Delta R_M^2) = \lambda_0, \quad (11)$$

$$b = \frac{\lambda_0 - a\Delta R_M}{\Delta R_M(2R_M - \Delta R_M)}. \quad (12)$$

Conversely, in the center part, the diffraction condition is as follows:

$$\phi_d(r_1) = \frac{2\pi}{\lambda_0}(ar_1) = \frac{2\pi}{\lambda_0}(a\Delta R_1) = 2\pi, \quad (13)$$

$$a = \frac{\lambda_0}{\Delta R_1}. \quad (14)$$

Because of diffraction limitation, ΔR_M is greater than the wavelength of incident light. In contrast, ΔR_1 is not made so large as to prevent the transmission of the zeroth-order light in the lens structure. The relationship between the phase shifts, ϕ_d and r , is shown in Fig. 2(a). From Eq. (2), the phase shift of the grating structure becomes increasingly linear as r_m increases. Conversely, the phase shift of the diffractive lens structure increases parabolically as r_m increases. These phase shifts are summed to yield the phase shift of the designed binary diffractive lens as shown in Fig. 2(a). The center part of the binary diffractive lens structure resembles a grating structure, while the outer part resembles a diffractive structure.

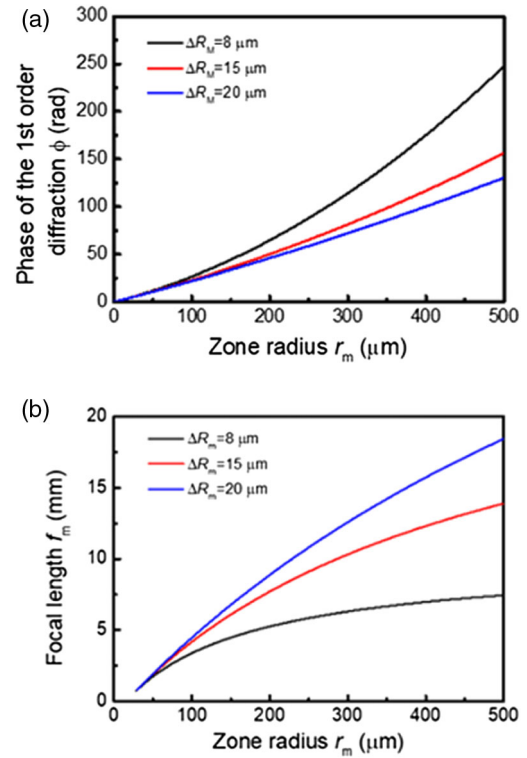


Fig. 2. Relationship between the zone radius and the phase of the first-order (a) diffraction and (b) focal length.

The light path difference from the annular zone of P_m and P_{m-1} for r_m and r_{m-1} , respectively, is consistent with Eq. (15). Therefore, the focal length f_m for the annular zone interval $\Delta r_m = r_m - r_{m-1}$ is obtained from Eq. (17). The focal length for each annular zone, determined using Eq. (17), is ascertained using r_m , r_{m-1} , and λ_0 . However, the focal depth depends on the value of b as shown in Eq. (12), and the value of b is determined using R_M , ΔR_1 , ΔR_M , and λ_0 . The values of R_M , ΔR_1 , and ΔR_M are determined; following this, all the structures in the lens are determined. Therefore, the focal length and the depth of the focus are not independently determined. Figure 2(b) shows the relationship between the focal length and zone radius. When $\Delta R_M = 8 \mu\text{m}$, the focal length is almost constant (6.8 mm) in the outer zone radius. Conversely, when $\Delta R_M = 15 \mu\text{m}$ and $20 \mu\text{m}$, the focal length gradually increases with the zone radius. From these results, it can be inferred that the effect of the diffractive lens is stronger for small values of ΔR_M ;

$$P_m - P_{m-1} = \lambda_0, \quad (15)$$

$$(f_m + r_m)^{\frac{1}{2}} - (f_m + r_{m-1})^{\frac{1}{2}} = \lambda_0, \quad (16)$$

$$f_m = \frac{1}{2\lambda_0} \sqrt{(r_m^2 - r_{m-1}^2)^2 - 2\lambda_0^2(r_m^2 + r_{m-1}^2) + \lambda_0^4}. \quad (17)$$

B. Simulation Results

We performed simulations using the three-dimensional fast Fourier transform beam-propagation method (FFT-BPM)

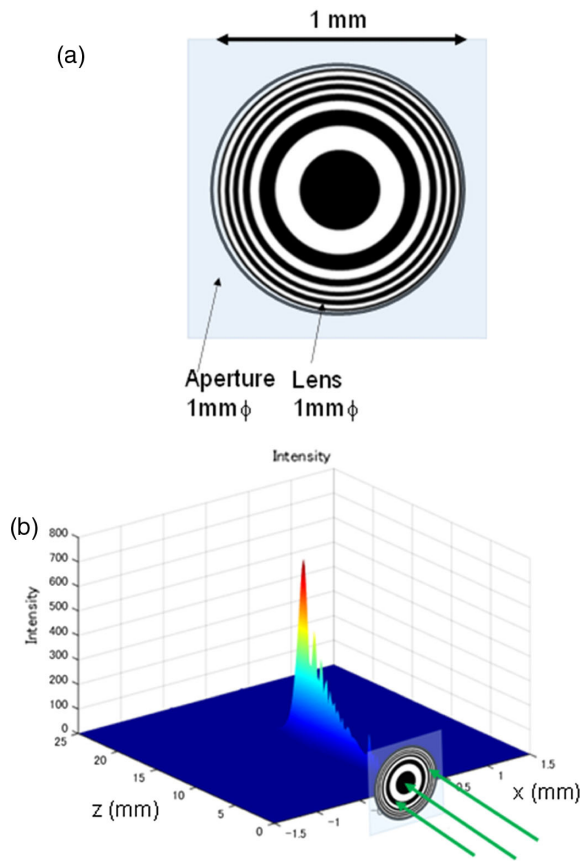


Fig. 3. Schematic diagram for (a) placement of lens and aperture and (b) example of the simulation result.

in MATLAB. This method involves solving the Helmholtz equation in paraxial approximation. Figure 3(a) shows the results of a three-dimensional simulation with the following parameters: $\Delta R_1 = 30 \mu\text{m}$, $\Delta R_M = 15 \mu\text{m}$, $\lambda_0 = 532 \text{ nm}$, and $R_M = 500 \mu\text{m}$. An aperture with a diameter of 1 mm was attached to the surface of the diffractive lens as shown in Fig. 3(a). We used a plane wave for the incident light. BPM simulation was performed for lens positions from $x = -0.5$ to 0.5 mm as indicated in Fig. 3(b) ($\Delta R_M = 15 \mu\text{m}$). The simulated lens was then observed to produce a strong intensity of propagation up to a distance of $z = 12.8 \text{ mm}$ at $x = 0 \text{ mm}$ by focusing. Beyond $z = 12.8 \text{ mm}$, at $x = 0 \text{ mm}$, the intensity rapidly decreases. In contrast, before $z = 12.8 \text{ mm}$, the intensity increases gradually with z at $x = 0 \text{ mm}$. This effect is due to Fresnel diffraction at the edge of the aperture. Detailed distributions in the z direction at $x = 0$ for different ΔR_M ($\Delta R_M = 8, 15, \text{ and } 20 \mu\text{m}$) are shown in Fig. 4(a). As shown in Fig. 3(b), there are strong peaks in the intensity distribution for each parameter ΔR_M , and the intensity distribution is left-right asymmetrical. For example, for $\Delta R_M = 15 \mu\text{m}$, the peaks are found at 12.8 mm. This is the focal point of the lens. Between $z = 0 \text{ mm}$ and $z = 12.8 \text{ mm}$, the intensity gradually increases with z owing to the effect of Fresnel diffraction at the edge of the aperture. These peaks attributed to the Fresnel diffraction are shown in Fig. 3(b). These peaks are not observed in Fig. 4(a) because they are significantly weaker than the other peaks ($\Delta R_M = 8 \text{ and } 20 \mu\text{m}$). Similar results are obtained for

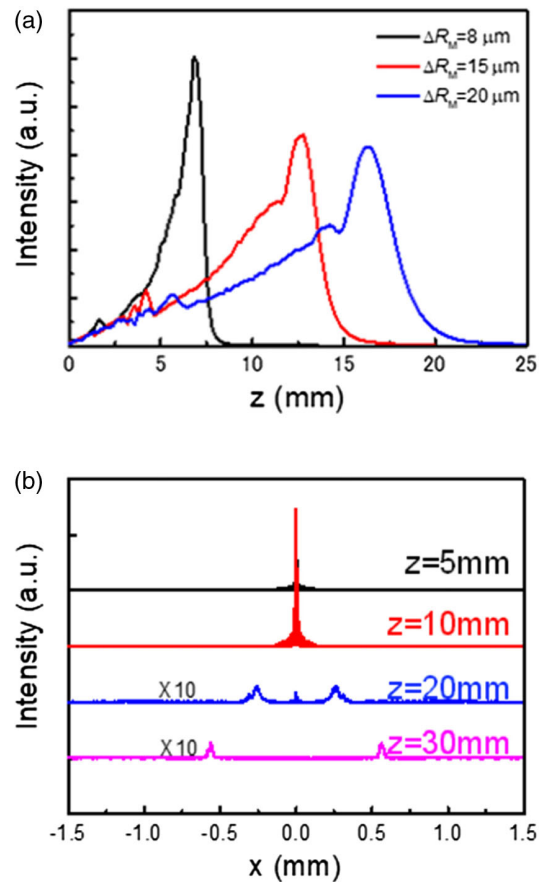


Fig. 4. Simulation results for the (a) z direction ($x = 0$) and (b) x direction.

$\Delta R_M = 8$ and $20 \mu\text{m}$. With increasing ΔR_M , the peak position is shifted further away from the lens. When $\Delta R_M = 8 \mu\text{m}$, a sharp peak is obtained. From these results, for $\Delta R_M = 8 \mu\text{m}$, the effect of the diffractive lens dominates that of the diffractive grating; thus, a sharp peak was obtained at 6.8 mm. However, for $\Delta R_M = 15$ and $20 \mu\text{m}$, the effect of the diffractive grating increases gradually; hence, wider distributions are obtained in the z direction. Figure 4(b) shows the intensity distribution in the x direction for $z = 5, 10, 20, \text{ and } 30 \text{ mm}$. For $z = 5$ and 10 mm , one peak is obtained on the optical axis.

However, for $z = 20$ and 30 mm , two peaks are obtained outside of the optical axis. The intensity of $z = 20$ and 30 mm is very weak; hence, the intensity distributions shown were magnified 10 times.

3. RESULTS AND DISCUSSION

A. Fabrication and Characterization

The substrates used were made of 1 mm thick quartz glass. Prior to spin-coating the electron-beam (EB) resist, hexamethyldisilazane (HDMS) was spin-coated on the surface of the quartz glass substrate to improve the adherence between the substrate and EB resist. The surface was spin-coated with an EB-positive resist (ZEON, ZEP-520A), after which prebaking was performed. Subsequently, charge-up prevention treatment

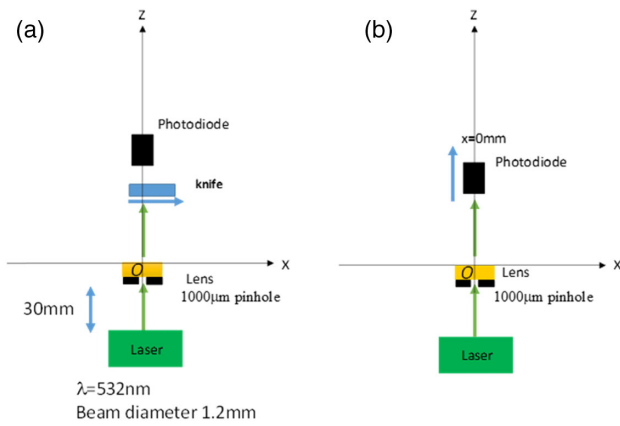


Fig. 5. Schematic diagram of the optical measurement in the (a) x direction and (b) z direction using a knife edge.

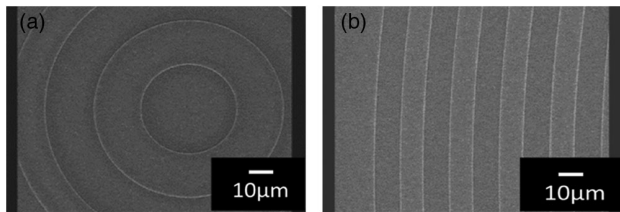


Fig. 6. SEM images of the (a) center and (b) edge regions.

was spin-coated on the EB resist. The electron-beam lithography (EBL) system (Crestec CABL-8000) was equipped with a ZrO/W thermal field-emission cathode. The acceleration voltage was 30 kV; electrons accelerated at this voltage were able to penetrate the resist. After exposure, the resist was developed, resulting in the binary diffractive lens. The size of the pattern for the binary diffractive lens was $1.0 \times 1.0 \text{ mm}^2$. Diffractive lenses fabricated by EBL with optimal characteristics, such as period, width, and height, are essential for fabricating the molds for thermal-type nanoimprint lithography.

Optical characteristics, such as the distribution of far-field transmitted intensity, were measured with a green laser ($\lambda = 532 \text{ nm}$) in the x direction and z direction as shown in Fig. 5. In the x direction, the knife-edge method was used to clearly measure the light distribution. A $1000 \mu\text{m}$ diameter pinhole was attached to the surface of the lens to align with the center of the lens to ensure that the incident light illuminates only the lens region. The resolutions for the x and z directions are 0.02 and 0.25 mm, respectively.

B. Experimental Results and Discussion

Figure 6 shows scanning electron microscope (SEM) images of both the center and edge of the prototype. The design values were $\Delta R_1 = 30 \mu\text{m}$ and $\Delta R_M = 15 \mu\text{m}$, while the measured values were $\Delta R_1 = 29.9 \mu\text{m}$ and $\Delta R_M = 15.0 \mu\text{m}$, confirming the precision of our fabrication process. In addition, lenses with design values of $\Delta R_M = 8 \mu\text{m}$ and $\Delta R_M = 20 \mu\text{m}$ were fabricated. The film thickness of the resist was measured using a noncontact film thickness monitor as 555 nm.

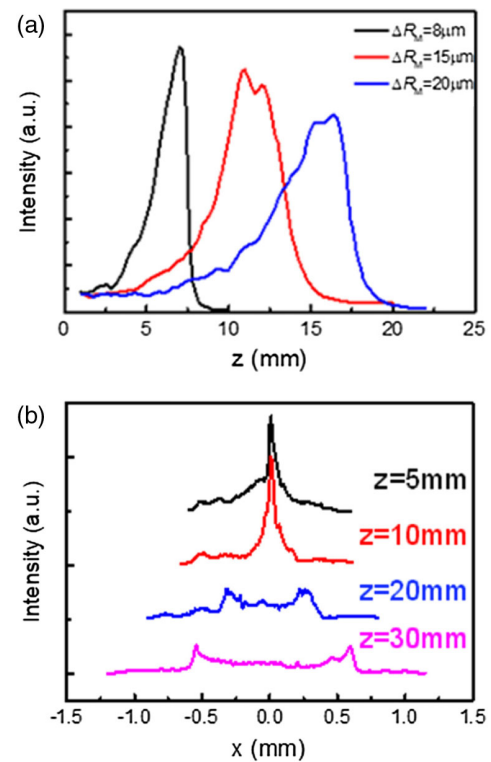


Fig. 7. Experimental results for the (a) z direction ($x = 0$) and (b) x direction ($\Delta R_M = 15 \text{ mm}$).

A green laser with a beam diameter of 1.2 mm was used as the light source to measure the light distribution. The measurements in the z direction involved attaching a $50 \mu\text{m}$ pinhole to the photodiode. Figure 7(a) shows a superimposition of the intensity distributions in the z direction for three lenses with $\Delta R_M = 20, 15,$ and $8 \mu\text{m}$. Two peaks were observed in the asymmetric profile, similar to that obtained in Fig. 3(c). The peaks at 16.4, 12.0, and 7.0 mm represent the focal points of the fabricated lens for $\Delta R_M = 20, 15,$ and $8 \mu\text{m}$, respectively. The peak shifts further away from the lens as ΔR_M increases. This result suggests that the focal length depends on ΔR_M . The other peaks are considered to be due to the Fresnel diffraction of the aperture. In the knife-edge method, the knife was placed in a plane perpendicular to the optical axis, and the intensity was measured while the knife was moved 10 mm in the x direction. As the system for measuring the light distribution is an integral system, the actual spatial intensity distribution can be obtained by differentiating with respect to the displacement of the knife. The measurements were performed by changing the distance between the knife and the lens to $z = 5, 10, 20,$ and 30 mm . Figure 7(b) shows the intensity distribution of the sample in the x direction ($\Delta R_M = 15 \mu\text{m}$). For all structures, the measurement results are consistent with the peak position of the simulation results.

From these results, it is considered that these intensity distributions, which are asymmetric spectra in the z direction, are formed by the overlapping of the peaks due to light focusing of the diffractive lens and Fresnel diffraction of the aperture. The former peak position can be controlled by the structure of the lens as shown in Fig. 2(b). For $\Delta R_M = 8 \mu\text{m}$, the peak

position is nearly constant because of the nearly constant phase distribution; thus, a sharp peak was obtained. Conversely, for $\Delta R_m = 15$ and $20 \mu\text{m}$, the peak position is gradually changed by the diffraction of each structure; thus, a broad peak can be obtained because the phase shift is gradually varied by the ring radius. In Fig. 7(a), two peaks are present, which correspond to the peak and shoulder in Fig. 4(a). The peak is the focal point of the lens, while the shoulder arises from Fresnel diffraction of the edge of the aperture. Therefore, we have confirmed that the intensity distribution on the optical axis can be realized by changing the structure of the lens. Because of the peak that resulted from Fresnel diffraction, the full width at half-maximum cannot be obtained. A method to eliminate the peak due to Fresnel diffraction needs to be studied in the future.

4. CONCLUSIONS

We realized a binary diffractive lens that can control focus distribution through phase shift achieved with a diffractive lens and diffractive grating. The lens structure was simulated using the three-dimensional FFT-BPM method. We investigated changes in intensity distribution along the z axis with respect to changes in the ring zone interval ΔR_M at the end of the lens. Our measurement results confirmed a strong intensity at $x = 0$ mm. With increasing ΔR_M , the peak position at $x = 0$ mm shifts further away from the lens. These results demonstrate that the intensity distribution on the optical axis could be controlled with a single flat lens by changing the periodic structure of the lens. We fabricated the lenses in this study by developing EB resist as a proof of concept; however, to apply the lenses to practical laser processing, lenses made of SiO_2 glass need to be fabricated using the dry etching process. Furthermore, to fabricate a lens for UV light from sources such as an excimer laser ($\lambda = 248, 193,$ and 157 nm) and fourth- or fifth-order harmonic YAG laser ($\lambda = 266$ and 213 nm), finer patterns less than $1 \mu\text{m}$ in dimension are needed.

Funding. Amada Foundation (AF-2017213); Japan Society for the Promotion of Science, KAKENHI (15H03556, 26390082).

Acknowledgment. We thank Prof. Hideto Miyake of Mie University for useful discussions. We also thank Enago (<https://www.enago.jp>) for English language editing.

Disclosures. The authors declare no conflicts of interest.

REFERENCES

1. A. Motogaito and K. Hiramatsu, "Fabrication of binary diffractive lens on optical films by electron beam lithography," in *Advances in Unconventional Lithography* G. Kostovski, ed., (In Tech, 2011), pp. 139–148.
2. J. L. Soret, "Concerning diffraction by circular gratings," *Ann. Phys. Chem.* **232**, 99–113 (1875).
3. L. B. Lesem, P. M. Hirsch, and J. A. Jordan, Jr., "The kinoform: a new wavefront reconstruction device," *IBM J. Res. Dev.* **13**, 150–155 (1969).
4. J. A. Jordan, Jr., P. M. Hirsch, L. B. Lessem, and D. L. Van Rooy, "Kinoform lenses," *Appl. Opt.* **9**, 1883–1887 (1970).
5. G. J. Swason and W. B. Veldkamp, "Diffractive optical elements for use in infrared systems," *Opt. Eng.* **28**, 605–608 (1989).
6. Y. Orihara, W. Klaus, M. Fujino, and K. Kodate, "Optimization and application of hybrid-level binary zone plates," *Appl. Opt.* **40**, 5877–5885 (2001).
7. K. Yamada, W. Watanabe, Y. Li, and K. Itoh, "Multilevel phase-type diffractive lenses in silica glass induced by filamentation of femtosecond laser pulses," *Opt. Lett.* **29**, 1846–1848 (2004).
8. P. Lalanne, S. Astilean, P. Chavel, E. Cambriil, and H. Launois, "Design and fabrication of blazed binary diffractive elements with sampling periods smaller than the structural cutoff," *J. Opt. Soc. Am. A* **16**, 1143–1156 (1999).
9. P. Lalanne, "Waveguiding in blazed-binary diffractive elements," *J. Opt. Soc. Am. A* **16**, 2517–2520 (1999).
10. B. H. Kleemann, M. Seesselberg, and J. Rudoff, "Design concepts for broadband high-efficiency DOEs," *J. Eur. Opt. Soc.* **3**, 08015 (2008).
11. A. Motogaito, N. Machida, T. Morikawa, K. Manabe, H. Miyake, and K. Hiramatsu, "Fabrication of a binary diffractive lens for controlling the luminous intensity distribution of LED light," *Opt. Rev.* **16**, 455–457 (2009).
12. A. Motogaito and K. Hiramatsu, "Fabrication of binary diffractive lenses and the application to LED lighting for controlling luminosity distribution," *Opt. Photon. J.* **3**, 67–73 (2013).
13. Y. Matsuoka, Y. Kizuka, and T. Inoue, "The characteristics of laser micro drilling using a Bessel beam," *Appl. Phys. A* **84**, 423–430 (2006).
14. Y. Kizuka, M. Yamauchi, and Y. Matsuoka, "Characteristics of a laser beam spot focused by a binary diffractive axicon," *Opt. Eng.* **47**, 053401 (2008).
15. A. Sabatyan and S. A. Hoseini, "Diffractive performance of a photon-sieve-based axilens," *Appl. Opt.* **53**, 7331–7336 (2014).
16. N. Davidson, A. A. Friesem, and E. Hasman, "Holographic axilens: high resolution and long focal depth," *Opt. Lett.* **16**, 523–525 (1991).
17. J. Sochacki, S. Bara, Z. Jaroszewicz, and A. Kolodziejczyk, "Phase retardation of the uniform-intensity axilens," *Opt. Lett.* **17**, 7–9 (1992).
18. A. Vijayakumar and S. Bhattacharya, "Design of multifunctional diffractive optical elements," *Opt. Eng.* **54**, 024104 (2015).
19. K. Huang, F. Qin, H. Liu, H. Ye, C.-W. Qiu, M. Hong, B. Luk'yanchuk, and J. Teng, "Planar diffractive lenses: fundamentals, functionalities, and applications," *Adv. Mater.* **30**, 1704556 (2018).
20. P. Wang, N. Mohammad, and R. Menon, "Chromatic-aberration-corrected diffractive lenses for ultrabroadband focusing," *Sci. Rep.* **6**, 21545 (2016).
21. C. Williams, Y. Montelongo, and T. D. Wilkinson, "Plasmonic metalens for narrowband dual-focus imaging," *Adv. Opt. Mater.* **5**, 1700811 (2017).
22. C. Zheng, H. Zang, Y. Du, Y. Tian, Z. Ji, J. Zhang, Q. Fan, C. Wang, L. Cao, and E. Liang, "Realization of arbitrarily long focus-depth optical vortices with spiral area-varying zone plates," *Opt. Commun.* **414**, 128–133 (2018).
23. P. Lalanne and P. Chavel, "Metalenses at visible wavelengths: past, present, perspectives," *Laser Photon. Rev.* **11**, 1600295 (2017).
24. E. Arbabi, A. Arbabi, S. M. Kamali, Y. Horie, M. Faraji-Dana, and A. Faraon, "MEMS-tunable dielectric metasurface lens," *Nat. Commun.* **9**, 812 (2018).